

TIME-LAPSE SEISMIC OF THE SUBSURFACE UNDERLYING A DYNAMIC OCEAN

M. Werning and D. Gajewski

email: michaela.werning@zmaw.de

keywords: Time-lapse, seismic, dynamic ocean, repeatability

ABSTRACT

Time-lapse seismic has become ever more important to monitor targets that lie in ever increasing depths. The difference between two or more seismic sections acquired with a certain time interval can be used to obtain information on the variation of geophysical properties in a reservoir. There are several factors influencing the results of time-lapse seismic data. The successful application of 4D techniques depends on the strength and size of the 4D signal compared to the background noise. In the analysis of time-lapse data, even travel time variations as small as 1 m/s can have an impact on the data by masking the real signature or introducing artifacts. Besides the change in geophysical properties, a multitude of other factors can produce differences. One of the greatest challenges are changes in the water column between different surveys. These changes can occur between different vintages but they can also significantly affect the acquisition of a single survey. Especially for deep water surveys the cumulative distortions due to variations in water velocity can reduce the imaging accuracy and lead to time shifts of up to several milliseconds. If these variations in water velocity remain undetected, the increasing or decreasing travel times in the pre-stack data affect the CMP gathers and the velocity analysis as well as the imaging. In this work, the influence of a dynamic ocean on time-lapse seismic data is investigated using synthetic data. Difference sections reveal that a dynamic ocean has indeed an impact on the seismic data. Furthermore, using a dynamic water column introduces NRMS errors of up to 60% to the data which is much higher than the NRMS values normally achieved nowadays. Cross-correlations reveal lags of 2 ms in time as well as lags of 2 CMPs in space. The broader the frequency spectrum used for all these analysis techniques, the more distinct are the differences; emphasising the fact that broadband signals allow the detection of subtle 4D differences.

INTRODUCTION

Over the last decades, reservoirs have become harder to find and the targets that are now in the focus of the seismic exploration industry lie in increasing depths. Due to these factors, time-lapse or 4D seismic data has become an important tool, especially for the monitoring of already existing reservoirs where it can serve as a partial substitute for drilling (Vedanti et al., 2009). For time-lapse or 4D seismic, seismic data for a certain acquisition area is recorded at different time intervals (the 4th dimension stands for the calendar time). The time gaps between the different recordings (also called vintages) can range from hours separating subsequent boat passes to months or years (MacKay et al., 2003). The difference between the acquired vintages can be used to obtain information on the variation of geophysical properties in the reservoir, for example due to hydrocarbon production (Vedanti et al., 2009). The information provided by 4D seismic data can be separated into two categories: travel time changes (time shifts) and amplitude changes between the first survey (also often called baseline survey) and the following surveys (also called monitor surveys) (Vedanti et al., 2009; Evensen and Landrø, 2010). Whereas the changes in amplitude result from local changes close to the interfaces, the changes in travel time for a specific horizon are due

to changes located along the ray path. These are either caused by a change in the distance the signal has to travel or by a change in the acoustic velocity (Evensen and Landrø, 2010). There are several factors influencing the results of time-lapse seismic data. The successful application of 4D techniques depends on the strength and size of the 4D signal compared to the background noise. This signal, in turn, depends on the rock and fluid properties (Marsh et al., 2003). In the ideal case of monitoring a reservoir, the differences between the seismic images of the different vintages will only occur within the area of the reservoir zone due to the production in the time interval between the surveys (Rickett and Lumley, 2001). In the real world, however, differences in the images are often visible throughout the entire dataset, including zones where presumably no changes occurred (Rickett and Lumley, 2001).

These other differences can be generated by a multitude of different sources and in the worst case, the effects of these sources may be much stronger than the signature of the production-related 4D differences making the interpretation of time-lapse data sets for reservoir analysis misleading or futile (Spetzler and Kvam, 2006; Rickett and Lumley, 2001). The most important factor influencing the results of time-lapse seismic is the repeatability of the different vintages. There are several reasons for non-repeatability issues in marine seismic acquisition: differences in the air gun-hydrophone response, seasonal changes in water temperature, tidal differences, etc. (Spetzler and Kvam, 2006). Several authors have shown in repeatability studies that even small changes in tides, water table, ambient noise conditions, source and receiver positioning etc. can have significant effects on 4D seismic data (Vedanti et al., 2009). Although some repeatability problems can be addressed by carefully planning the 4D acquisition design, the greatest challenge in the marine acquisition of time-lapse data is the change in physical ocean properties of the water column, which may need to be addressed in the time-lapse data processing (MacKay et al., 2003; Lacombe et al., 2009; Vedanti et al., 2009). These changes can occur between different vintages but they can also significantly affect the acquisition of a single survey. Seawater velocity variations are a critical issue in time-lapse seismic data since they can perturb the amplitude and travel time. Therefore a suitable quantitative analysis of the time-lapse data might be impossible (Bertrand, 2005). The primary cause of dynamic velocity changes are changes in the water temperature resulting in a change of over 3 m/s per degree of water temperature (MacKay et al., 2003; Bertrand, 2005). The temperature and therefore the velocity in the water layer changes both laterally and vertically as well as with calendar time (Bertrand and MacBeth, 2003; Bertrand, 2005). The largest influence on seismic data is the seasonal variability as it can inflict velocity changes of up to 20 m/s anywhere between 100 m and 1000 m of water depth (Bertrand, 2005). In the analysis of time-lapse data, even variations as small as 1 m/s can have an impact on the data by masking the real signature or introducing artefacts. Especially for deep water surveys the cumulative distortions due to variations in water velocity can reduce the imaging accuracy and lead to time shifts of up to 10 – 30 ms (MacKay et al., 2003; Lacombe et al., 2009; Bertrand, 2005). The dynamic change of recorded travel time poses a problem for the comparison of different vintages (MacKay et al., 2003). If these variations in water velocity remain undetected, the increasing or decreasing travel times in the pre-stack data affect the CMP gathers and the velocity analysis. The performance of the velocity analysis is impaired and the coherency of the stack reduced. This, on the other hand, leads to time mis-positioning, lateral discontinuities, and amplitude variations in the post-stack data producing an imprint on the seismic data that can be misinterpreted as the indication of gas or other physical properties (Lacombe et al., 2009; MacKay et al., 2003). But the effects induced by seawater velocity variations cannot be easily removed by conventional processing techniques (Bertrand and MacBeth, 2003). Specific processes are needed to handle these variations (Bertrand, 2005).

Bertrand and MacBeth (2005) investigated the impact of seawater velocity variations on time-lapse data by using a zero-lag time-lapse seabed experiment with no changes in the subsurface but velocity changes in the water-column ensuring that the changes recorded by the seismic data are caused only by the velocity changes. They used a constant velocity model (with a velocity of 1500 m/s) of the water column for the baseline survey and a heterogeneous water model for the repeat survey which was designed by using two vertical velocity profiles from measurements in the West of Shetlands area and interpolating between them. The difference between the two vintages showed amplitudes in the order of magnitude of the individual survey. Bertrand and MacBeth (2005) stated that the higher the velocity difference, the poorer the repeatability and the stronger the residual amplitude. For example, a difference in sea-water velocity of

10 m/s between both vintages could reduce the stacked amplitudes by up to 40% in some parts of the survey.

But the study done by Bertrand and MacBeth (2005) is just a partial representation of the real world. There is no such thing as a homogeneous ocean and even a heterogeneous ocean changes its physical properties with time. Therefore, the work of Bertrand and MacBeth (2005) is extended to investigate the influence of a dynamic ocean on time-lapse seismic data. For this purpose, different synthetic datasets were created using a 2D model of the Mediterranean outflow of the Strait of Gibraltar. By using synthetic data, a lot of the issues concerning time-lapse data can be avoided. Since the datasets are acquired in the exact same manner, all influences on the repeatability that are normally introduced by the acquisition of field data can be neglected, i.e. source and receiver positioning, variances in the acquisition area. This also simplifies the preprocessing of the data since no cross-equalization is needed to render the different datasets comparable. The influence of the dynamic water column on the results of the time-lapse data is investigated by comparing the seismic section of a static ocean model snapshot to the seismic section of the dynamic ocean model regarding the repeatability of the data.

CREATION OF THE SYNTHETIC DATA

The oceanic feature that was modelled for the creation of the synthetic datasets is the Strait of Gibraltar. This particular area was chosen based on its unique oceanographic characteristics. The large temperature and salinity contrasts between the Atlantic and the Mediterranean water masses are not only interesting from an oceanographic point of view but they also generate strong impedance contrasts compared to the remaining water column. Although these density contrasts are very small compared to the ones normally used in the seismic exploration, they are sufficient to be imaged by reflection seismic methods. Another fact that makes the Strait of Gibraltar a preferable study area from a seismic point of view are the high flow velocities of up to 0.5 m/s. The outflow of the Mediterranean Sea through the Strait of Gibraltar into the Gulf of Cadiz was originally modelled using a realistic 3D representation (Spickermann, 2011). For the generation of the synthetic data for this project a 2D version of the 3D representation was used which consists of 2D model snapshots with a time interval of 100 s. Included in the 2D version are the temporal variability of salinity, temperature, density, and therefore also the temporal variability in acoustic velocity.

Ocean model parameter	Value
Horizontal resolution	160 m
Vertical resolution	2 m
Temporal resolution	100 s
Horizontal extent	240 km
Depth	2 km
Acoustic velocity	1497 – 1526 m/s

Table 1: Ocean model parameters used for generating the synthetic datasets

As shown in Table 1 the variance between the minimum and maximum acoustic velocity is less than 2%. Therefore, the impedance contrasts generated by these velocity variations are also very small. The different water masses are clearly defined by their respective velocities. Whereas the Atlantic water shows velocities between 1498 to approximately 1511 m/s, the velocities of the Mediterranean water range from 1510 to 1525 m/s. The sub-seabed velocity was set to 1540 m/s which is close to the seawater velocities (see Fig. 1). Although this is not a realistic value for sub-seabed conditions, the value was chosen to avoid a strong sea bottom reflection which would influence the seismic imaging of the water column, which was the aim of the work of Raub (2011) where this datasets were used for the first time. For further investigations of the impact of the water on sub-seabed reflections, which is the focus of this work, the model was extended to a depth of 2240 m and three reflective interfaces were added. The first subsurface layer has the aforementioned velocity of 1540 m/s and is followed by a sinusoidal layer with a velocity of 1560 m/s. At the bottom of the sinusoidal layer, a reflector element with 45° ramp over a vertical extent of

150 m was added. The last reflector element, separated from the other elements by a layer with a velocity of 1540 m/s, is a horizontal reflector with a velocity of 1560 m/s. The marine survey designed to model the synthetic data sets spans a 26.96 km excerpt of the original ocean model. A ship movement of 4 knots was assumed which leads to a shot interval of 20 s and a total recording time of 208 min. The remaining survey parameters are presented in Table 2.

Survey parameter	Value
Number of shots	625
Shot spacing	40 m
Shot interval	20 s
Number of receivers	101
Receiver spacing	20 m
Minimum offset	0 m
Maximum offset	2000 m

Table 2: Survey parameters used for generating the synthetic datasets

The chosen survey parameters resulted in the acquisition of 2597 Common Mid Points (CMPs) with a CMP spacing of 10 m covering an excerpt of 25.96 km. The maximum CMP fold for this survey was 25, which is low compared to field data but sufficient when using synthetic data. The first shot was fired at a horizontal position of 1 km and a depth of 0 m. The first receiver channel was placed at the same depth at maximum offset and the receiver numbers increase with decreasing offset ending with channel 101 at the source location. The source wavelet for this marine survey was represented by a zero-phase Ricker wavelet with a dominant frequency of 60 Hz and a maximum frequency of 120 Hz. Assuming an acoustic velocity of 1500 m/s this results in a minimum wavelength of 12.5 m. A time sample interval of 1 ms was used.

The synthetic seismograms were modelled using the isotropic seismic modelling program Rapid Expansion Method in 2D (REM2D) which solves the acoustic and elastic wave equation directly and combines the rapid expansion method with the Fourier method (Kosloff et al., 1989). Due to the use of the Fourier method, Shannon's sampling theorem (at least two grid points per smallest wavelength are required) needs to be taken into account. Since the minimum wavelength used was 12.5 m, the acoustic velocity has to be interpolated from the original horizontal and vertical resolution of 160 m and 2 m respectively to a new horizontal and vertical resolution of 5 m to fulfil this theorem. A linear interpolation was used.

For generating a truly dynamic survey every shot had to be computed for the correct water model excerpt at the correct time step. Considering the temporal resolution of 100 s of the model and the shot interval of 20 s, five shots can be generated using the same snap shot of the model leading to a total of 125 snapshots for 625 shots. A double precision computation accuracy was required. For a detailed description of the scripts and methods used to generate the synthetic datasets please refer to Raub (2011) and Raub et al. (2012). Two different datasets are used in this work. One was computed using the dynamic model with the vessel moving against the outflow (from now on referred to as DYN) whereas the other one represents a snapshot of the dynamic model at the beginning of the recording (STAT, see Fig. 1). To remove the low-frequency tail of the direct wave, a Butterworth bandpass filter with the corner frequencies of 5, 40, 90, and 140 Hz was applied. The next step during the preprocessing was the application of an additional low-pass filter with corner frequencies of 10 and 60 Hz. This low-pass filter was introduced to suppress high frequency ringing and to enhance the water column reflections. To further enhance the water column reflections, the direct wave was removed from the synthetic data by using an eigenvector filter in ProMAX. A detailed description of this process can be found in Raub (2011) or Spickermann (2011). Since the Ricker wavelet used for generating the synthetic data is a zero-phase wavelet, the data needed to be shifted by the half wavelength of the Ricker wavelet, which corresponds to 25 ms for the maximum frequency of 120 Hz. Afterwards, the data was sorted to CMPs.

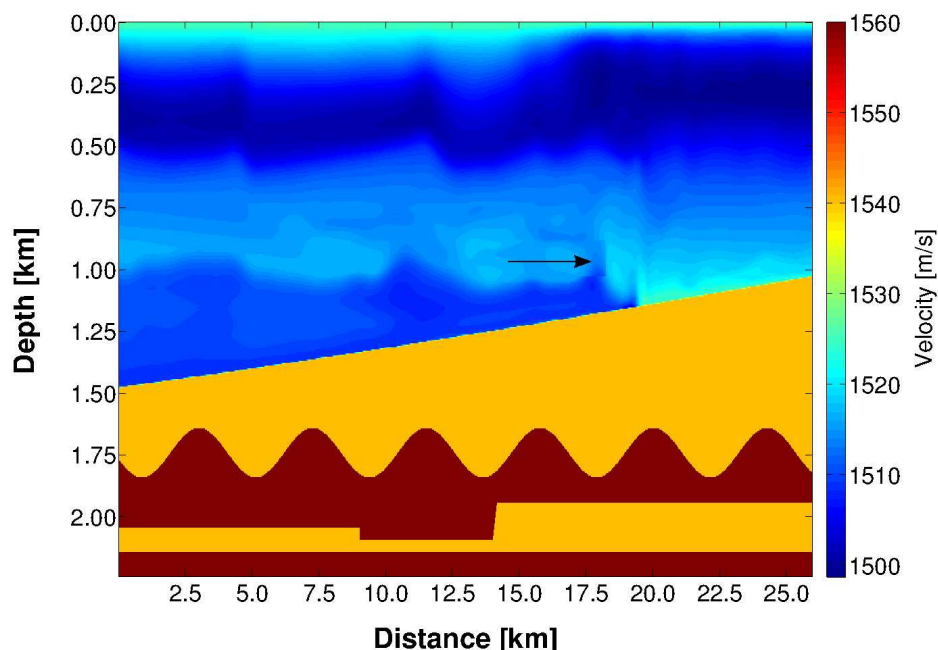


Figure 1: Snapshot of the 2D model at the beginning of the recording. Shown is the distribution of the acoustic velocity for the water column and the subsurface model. The black arrow marks a front of the Mediterranean water body moving six kilometres during the recording time.

Due to the results of the velocity analysis by Spickermann (2011), a constant stacking velocity of 1515 m/s was used in this work. The results for the two different datasets are shown in Fig. 2 and 3. Although stacking with a constant velocity is not a perfect representation for the entire water column, the key features analysed by Raub (2011) are still clearly visible. The area with the strongest resemblance between both datasets is on the left side where the acquisition of both datasets started.

Since the time intervals between subsequent 4D surveys are evermore decreasing in order to improve the dynamic characterization of reservoirs, the necessity to detect even smaller 4D signals, amplitude changes, and time shifts has arisen over the last years. Bertrand and Thiebaud (2008) and Yu and Thiebaud (2009) found that subtle 4D effects (smaller than 4 – 5 ms) are best detected by high-frequency data which will provide a more accurate time estimation and better time-lapse amplitudes. However, high-frequency time-lapse differences are also more sensitive to misalignments in time and therefore high-frequency time-lapse data is more affected by poor repeatability than low-frequency data. Since small time-lapse signals are expected in this work considering the small impedance contrasts in the data and no other sources except the water velocity variations influence the repeatability of the synthetic datasets, a second set of stacks from the synthetic data was created. To create these stacks, the Butterworth bandpass filter and the time shift mentioned earlier in this section were applied, but the additional low-pass filter and the direct wave removal were not applied. As the focus of this work is on the time-lapse signal of the subsurface generated by the velocity variations in the water column and not on the precise imaging of the water column reflections, it is not necessary to remove the direct wave for these datasets. The stacked sections for the datasets containing a broader frequency spectrum are shown in Fig. 4 and 5. Compared to the stacked seismic sections shown before, the high frequency content results in a better resolution of the subsurface structures. The resolution of the water column reflections are enhanced as well, but on the other side not all of them are recognisable in these sections due to the aforementioned high frequency ringing and the effects of the direct wave.

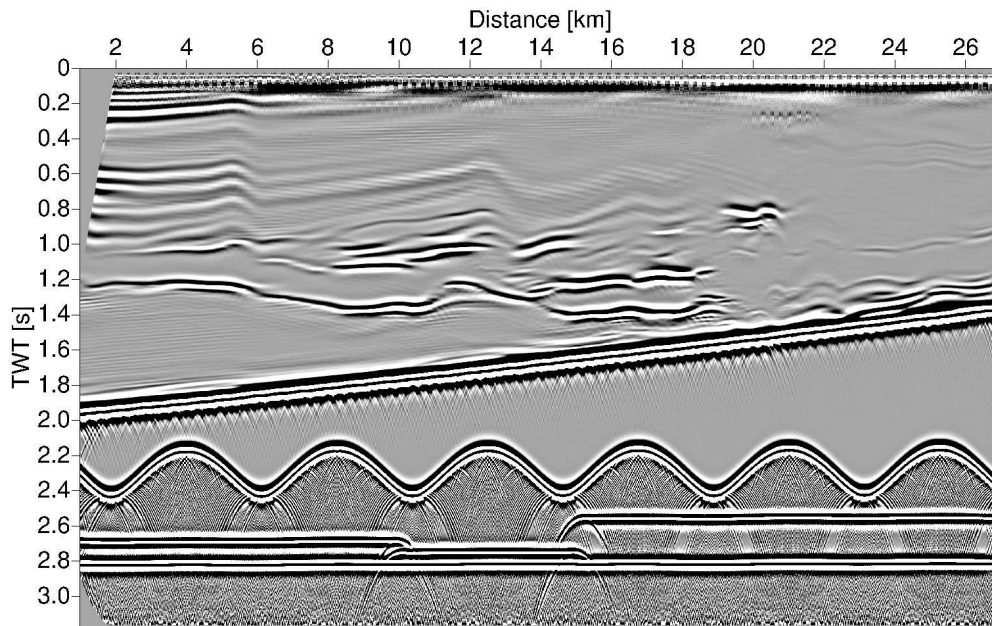


Figure 2: Brute stack of the dataset STAT from the beginning of the recording. A constant stacking velocity of 1515 m/s was used.

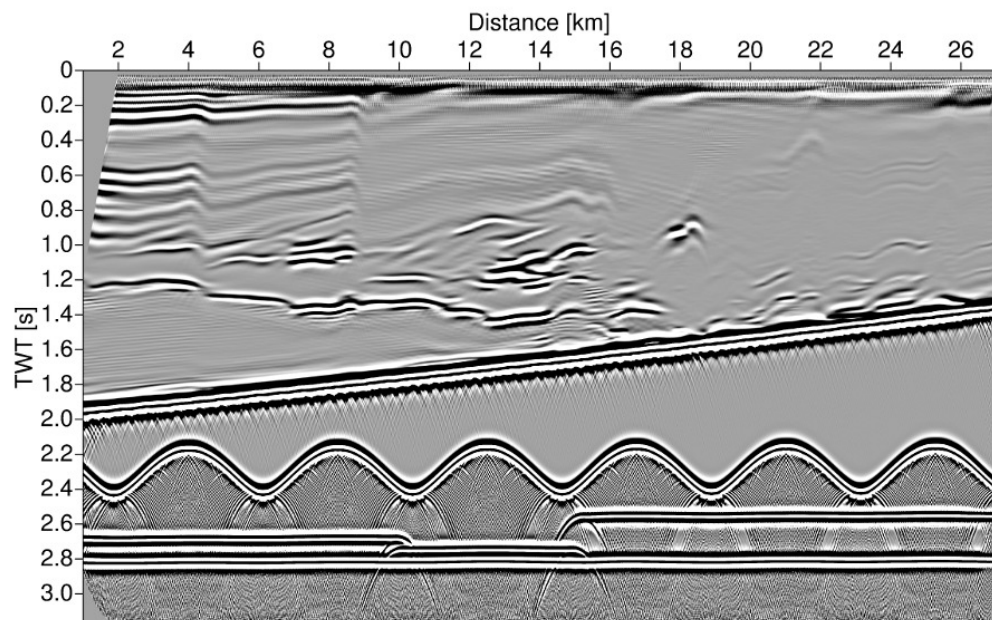


Figure 3: Brute stack of the dataset DYN recorded with the ship moving to the right. A constant stacking velocity of 1515 m/s was used.

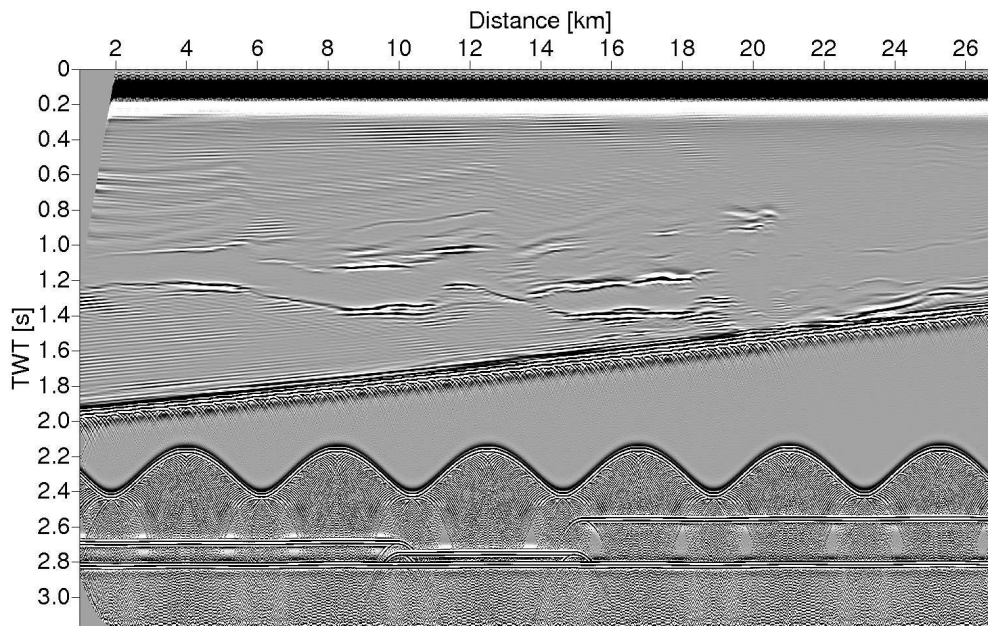


Figure 4: Brute stack of the dataset STAT from the beginning of the recording. A constant stacking velocity of 1515 m/s was used. Only the Butterworth bandpass filter and the phase shift were applied to the raw data, the removal of the direct wave and the additional low-pass filter were omitted.

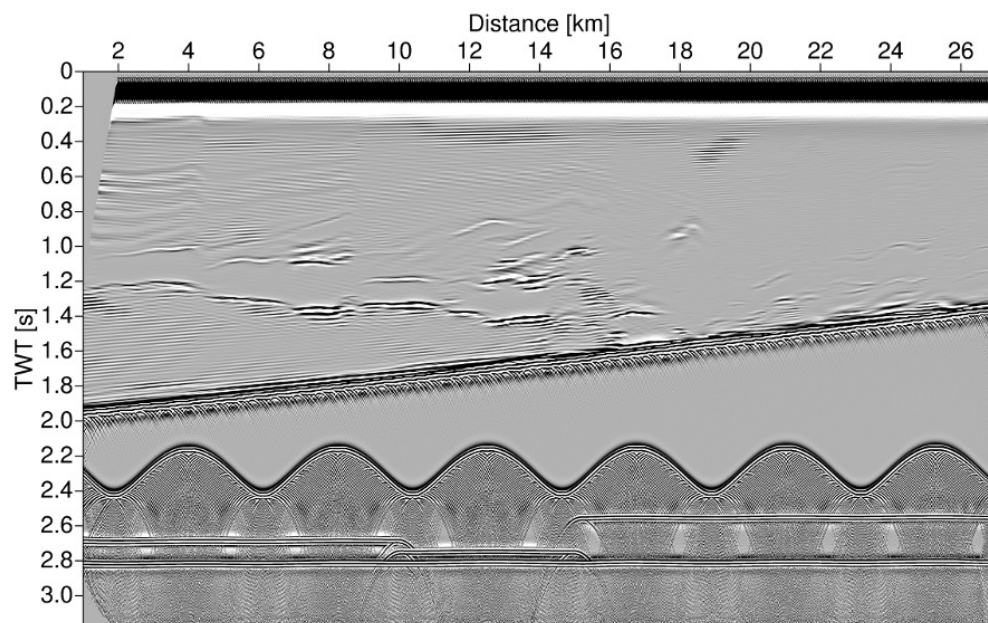


Figure 5: Brute stack of the dataset DYN recorded with the ship moving to the right. A constant stacking velocity of 1515 m/s was used. Only the Butterworth bandpass filter and the phase shift were applied to the raw data, the removal of the direct wave and the additional low-pass filter were omitted.

DIFFERENCES

In this section, the differences introduced by variations in the water column are assessed. This is done by creating difference sections, using 4D metrics and cross-correlations.

Subtraction

The first and easiest technique that comes to mind when thinking about the comparison between two datasets is to look at a difference section. In this difference section, the traces of the dynamic seismic section are subtracted from the static seismic section. The result is shown in Fig. 6. The largest differences between the two datasets can be seen in the middle part of the section between 10 and 20 km horizontal distance. There is also a small area of stronger differences around 4 km. Since STAT is a snapshot of the dynamic model at the beginning of the recording, there are no differences on the very left of the sections up to 4 km. The differences are most visible for the reflection of the sea bottom and the reflections of the subsurface structures whereas there are almost no or only very small differences in the water column. The location of the differences in this section correlates with the differences that are already visible with the bare eye when comparing the sections of DYN (Fig. 3) and STAT (Fig. 2). For example, for the area between 4 and 6 km strong differences between 1 and 1.2 s in the water column are visible when comparing DYN and STAT. The same is true for the differences between 10 and 20 km. Whereas the seismic section of STAT shows long lateral reflections in this area, the reflections in DYN are separated into several small reflections. There are just small differences in the water column between the two seismic sections for the area beyond 20 km which is also reflected in the difference section. The differences between the two sections are in the same order of magnitude of the amplitudes of the individual surveys which matches the results of Bertrand and MacBeth (2005). Although the differences in the water column between the sections are visible with the bare eye, the differences in the subsurface structures are only recognisable in the difference section.

The difference section is also computed for the datasets where no additional low-pass filter is applied to the data. The result is shown in Fig. 7. The same colour scale was used for all the difference plots. Compared to the one shown before, the difference section for the datasets where the additional low-pass filter was omitted shows more and stronger differences. The differences for the sea bottom reflection span over the whole section with just a few exceptions. Furthermore, differences are now recognisable for all of the subsurface structures and they are much stronger than in the previous examples. The trends discussed for Fig. 6 are also visible in this difference sections, but the differences in the water column are higher and better recognisable.

So far the differences were discussed in a qualitative way. To have a more quantitative description of the differences, the Normalized Root Mean Square values are analysed in the next section.

NRMS

As mentioned in the introduction, there are a multitude of sources generating residual differences in the repeated surveys that are not related to the changes in the reservoir. Bertrand and Thiebaud (2008) state that repeatability is the most important factor for a successful 4D experiment and that subtle 4D changes can only be detected with sufficient repeatability. Otherwise, 4D experiments normally fail. The metric most commonly used to quantify the repeatability of time-lapse data is the Normalized Root Mean Square (NRMS) difference of two traces, a and b , within a given time window $t_1 - t_2$ (Kragh and Christie, 2002; Stein et al., 2006). The NRMS value generated by dividing the RMS of the difference of both traces by the average RMS of the inputs is conventionally given in percentage and is defined by (Kragh and Christie, 2002)

$$NRMS = \frac{200 * RMS(a_t - b_t)}{RMS(a_t) + RMS(b_t)} \quad (1)$$

where the RMS operator is given by

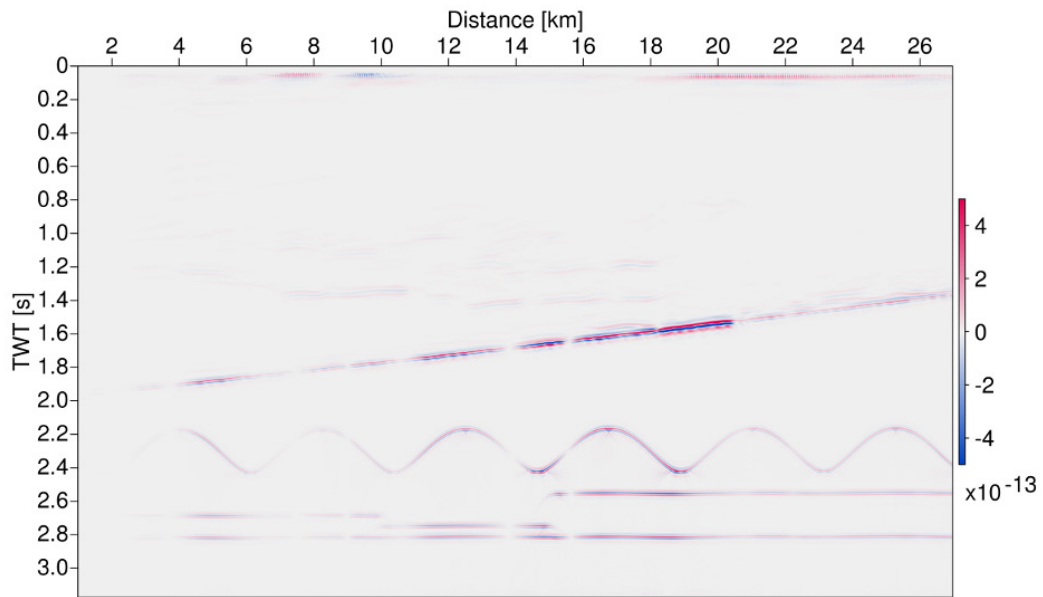


Figure 6: Difference section of the brute stacks of the dynamic dataset DYN and the static dataset STAT, which represents a snapshot of the dynamic model at the beginning of the recording.

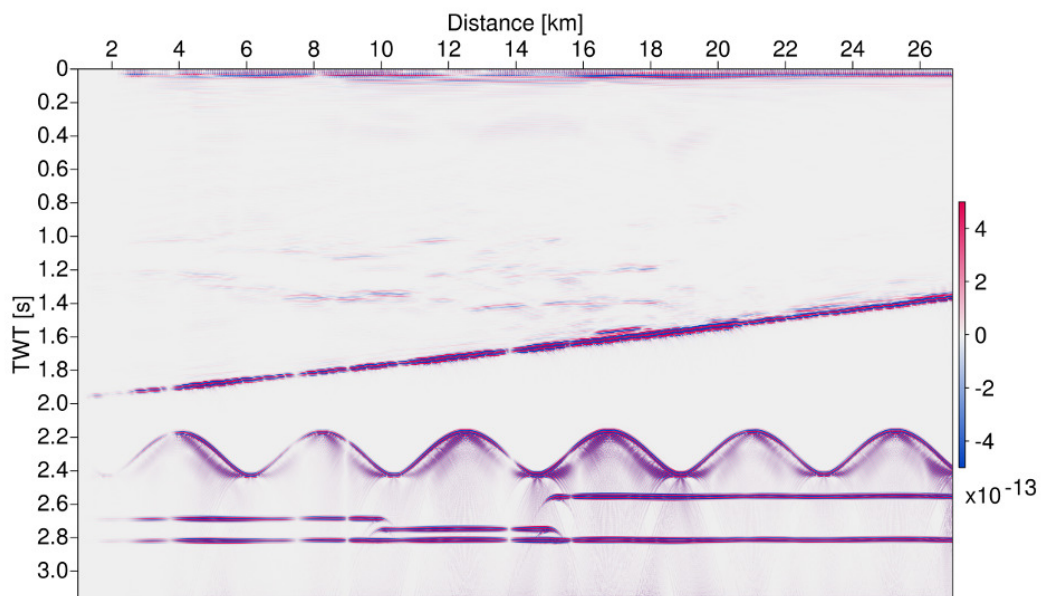


Figure 7: Difference section of brute stacks of the dynamic dataset DYN and the static dataset STAT which represents a snapshot of the dynamic model at the beginning of the recording. In this case, the additional low-pass filter and the removal of the direct wave were omitted.

$$RMS(x_t) = \sqrt{\frac{\sum_{t_1}^{t_2} (x_t)^2}{N}} \quad (2)$$

Although the NRMS values are given in percentage, the values are not intuitive since they are not limited to the range of 0 – 100% and the theoretical maximum is 200% (Kragh and Christie, 2002; Vedanti et al., 2009). For example, in the case of random noise in both traces the NRMS value is 141%. If one trace is half the amplitude of the other, the NRMS value is 66.7% and the NRMS error would reach its maximum value if one of the traces contained only zeros or both traces would anti-correlate.

There are several examples of NRMS values in the literature and the definition of a good or bad NRMS value changes from author to author. One trend that can be observed is that the NRMS values are decreasing with time and with improving acquisition technology. In recent 4D studies the NRMS value could be reduced to 10 – 30% (Vedanti et al., 2009). Stein et al. (2006) defined a NRMS value of above 50 – 60% as too large to be of real value and considered 20 – 40% as good whereas everything below 30% would be excellent values. This statement is matched by Houck (2007) who states that surveys with average NRMS differences of less than 20% have become common and that cases have been reported where a NRMS error below 10% was achieved.

Several studies were already conducted to assess the effect of different parameters on the repeatability. Laws and Kragh (2002) investigated the effect of rough seas in 4D seismic experiments. For a typical seismic line with a 48-fold stack, a 2 m difference in sea-state height (corresponding to a relatively calm sea) leads to a change in the 4D NRMS values of 5 – 10%.

Kragh and Christie (2002) investigated the influence of streamer positioning on the repeatability of time-lapse seismic data. Although the data are visually very repeatable, the NRMS error introduced by the positioning error reached surprisingly high values of 100% and more.

Bertrand and MacBeth (2005) found in their study that the difference between the two vintages led to quite high NRMS errors of 60 – 80%. This poor repeatability, however, could be reduced to quite constant NRMS values of 3% and below by applying a new dynamic correction specifically developed for permanent installations which removes the effect of seawater velocity variations.

For this work, an algorithm to calculate the NRMS error was implemented in Matlab. For most of the figures shown, just the part of the synthetic datasets between 2 and 3 s (TWT) is windowed since the emphasis of this work is on the subsurface structures.

Fig. 8 shows the NRMS values for the comparison of the dynamic and static dataset. The NRMS error ranges from 0 to approximately 50%. For a better comparison, the corresponding difference section is plotted in the upper part of Fig. 8. On the very left side of the seismic section, the NRMS value is very low with values under 10%. This correlates with the differences between the two datasets which are almost non-existing in this part since STAT is the snapshot of the dynamic model at the beginning of the recording. The NRMS error reaches 20% for the first time at approximately 3 km. At this point, the first larger differences are visible in the difference section. Although these differences continue up to 5 km, the NRMS value slowly declines until reaching almost 0% shortly before 7.5 km. Two broader peaks of approximately 10 and 25% follow before the NRMS value reaches its maximum values of 40 to 50% for three adjacent peaks between 13 and 18 km. These peaks correlate with strong differences in the seismic sections. Shortly before 15 km, a local minimum of approximately 5% occurs. In the difference section, this value coincides with a small interruption between two areas of large differences where almost no difference is recognisable. The right side of the section is dominated by smaller differences and therefore smaller NRMS errors of around 20%.

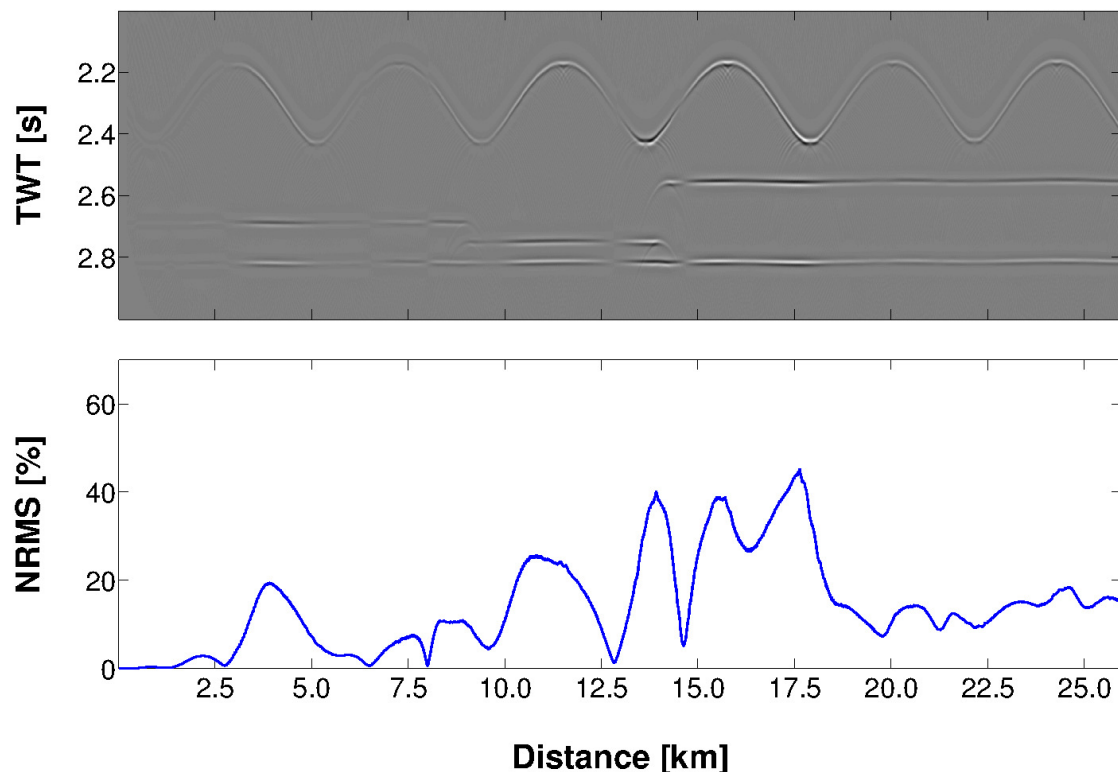


Figure 8: NRMS errors calculated for the datasets DYN and STAT and for the excerpt of the seismic section containing the subsurface reflections. In the upper part of this figure, the corresponding difference section is shown whereas the resulting NRMS value is presented in the lower part.

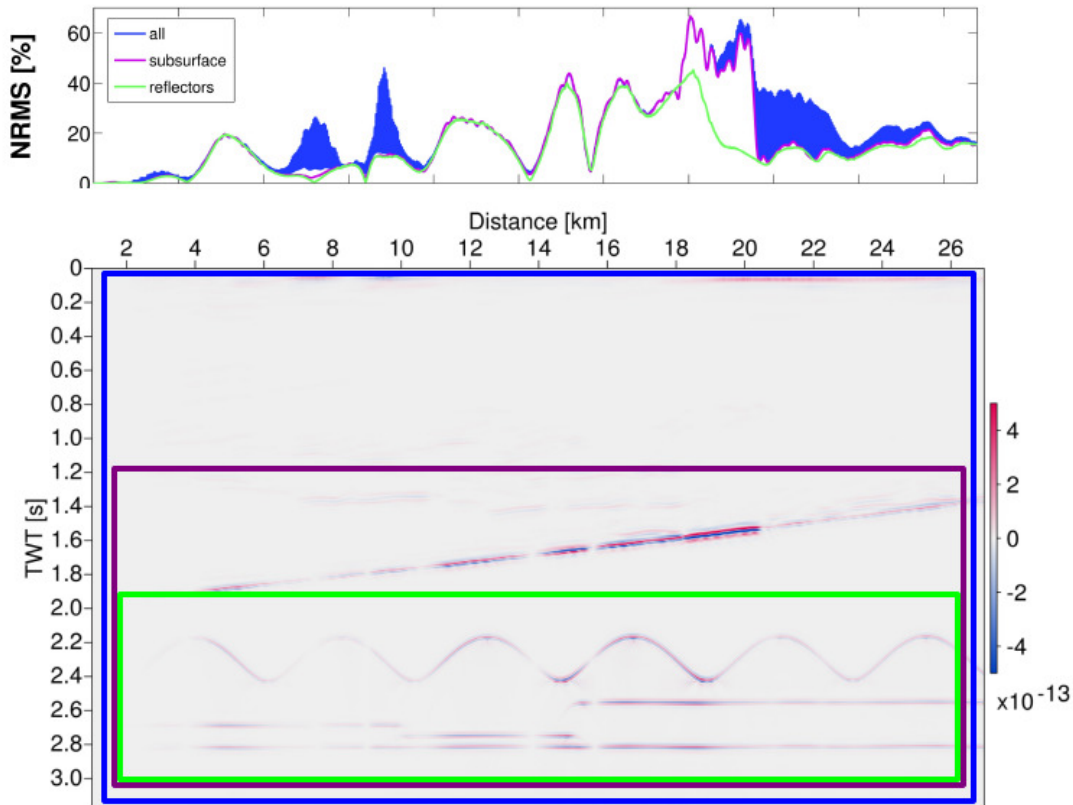


Figure 9: Comparison of the NRMS values for different excerpts of the synthetic datasets. The blue curve represents the NRMS error curve for the entire dataset. The violet curve represents the NRMS values for part of the water column and the subsurface reflections. The results for the excerpt containing only the subsurface reflections is shown in green.

The NRMS values for different excerpts of the seismic sections are shown in Fig. 9. The blue curve of this figure shows the NRMS value for the whole dataset including the water column. The violet curve includes just a part of the water column as well as the sea bottom and the subsurface reflections (1.2 – 3.0 s TWT), whereas the green curve only shows the NRMS errors for the excerpt containing the subsurface reflections. The maximum value for the subsurface reflections is approximately 40%, whereas it reaches values above 60% for the entire dataset. Furthermore, most of the largest peaks in the upper two images seem to be due to the reflection of the sea bottom since the values are much smaller for the area of the subsurface reflections (see for example the peaks between 17.5 and 20 km in Fig. 9). This matches the results of the difference sections shown in the previous paragraphs which showed strong differences for the sea bottom reflection.

The NRMS values of the datasets containing the high frequency part of the spectrum are shown in Fig. 10. The NRMS error curve shows the same behaviour as for the standard dataset (compare Fig. 8) with the exception that the NRMS values are significantly higher than in the previous case. Whereas the maximum NRMS error in Fig. 8 is approximately 50%, the maximum value in Fig. 10 is approximately 80%.

For the last test, random noise with a signal-to-noise ratio of 10 was added to the datasets before stacking. The corresponding NRMS values are shown in Fig. 11. Compared to Fig. 8, the NRMS errors in Fig. 11 are generally higher and around 40%. The curves in both images show the same trend (for

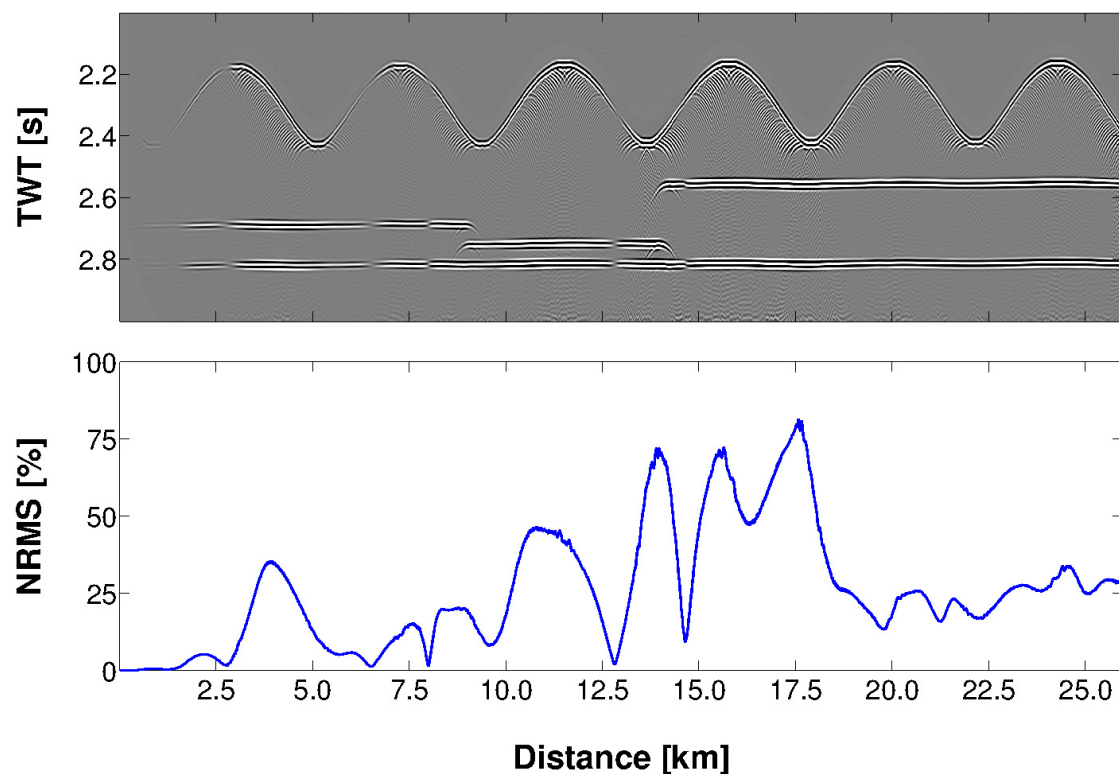


Figure 10: NRMS errors calculated for the datasets DYN and STAT and for the excerpt of the seismic section containing the subsurface reflections. For these datasets, the additional low-pass filter is not applied and the direct wave is still contained in the data. In the upper part of this figure, the corresponding difference section is shown whereas the resulting NRMS value is presented in the lower part.

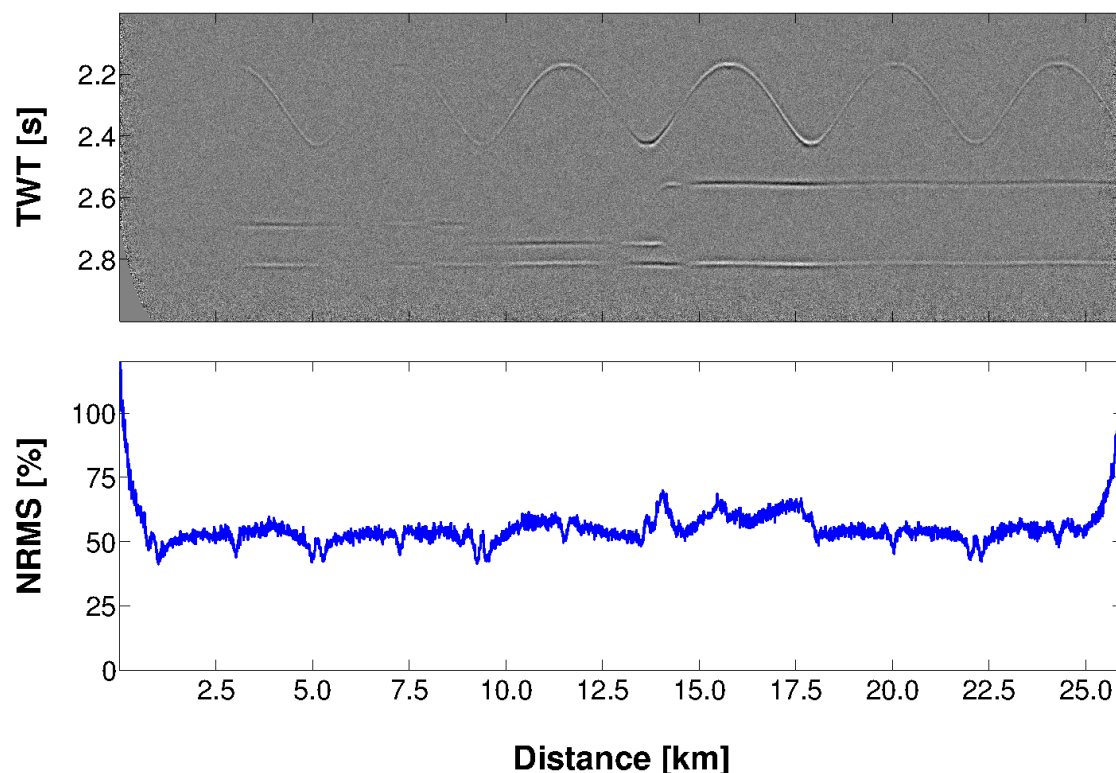


Figure 11: NRMS errors calculated for the datasets DYN and STAT and for the excerpt of the seismic section containing the subsurface reflections. Random noise with a signal-to-noise ratio of 10 was added to the data. In the upper part of this figure, the corresponding difference section is shown whereas the resulting NRMS value is presented in the lower part.

example the minima shortly after 2 km, before 10 km or at 20 km as well as the maxima between 12.5 and 17.5 km) but the difference between the peaks and the rest of the curve is decreased.

Cross-correlation

Another technique to compare two traces is cross-correlation. Cross-correlation can be used to determine the similarity of two traces. This is done by sample-wise multiplication of trace a and b. The cross-correlation was implemented in Matlab using the following equation

$$Coeff = \frac{ifft(fft(a) * conj(fft(b)))}{\sum a^2 * \sum b^2} \quad (3)$$

The zero-padded Fourier transformation of trace a is multiplied with the complex conjugate of the zero-padded Fourier transformation of trace b. The inverse Fourier transformation is performed on the result of that multiplication. The resulting product is then summed and normalized by dividing by the individual summations of the two input traces. This is also called 'normalized cross-correlation' and results in the cross-correlation coefficient. This coefficient is 1 for identical traces, -1 for traces that are the inverse of each other and small values close to zero for traces that are randomly dissimilar (Hill et al., 2006). By taking the maximum value of the result one gets the maximal similarity between the two traces and the corresponding lag for which this similarity is achieved. The cross-correlation is calculated using a window. For each sample of the dataset, the cross-correlation is calculated for shifts from -16 samples to

+16 samples around this position. This is done in the vertical (or time) as well as in the horizontal (or space) direction.

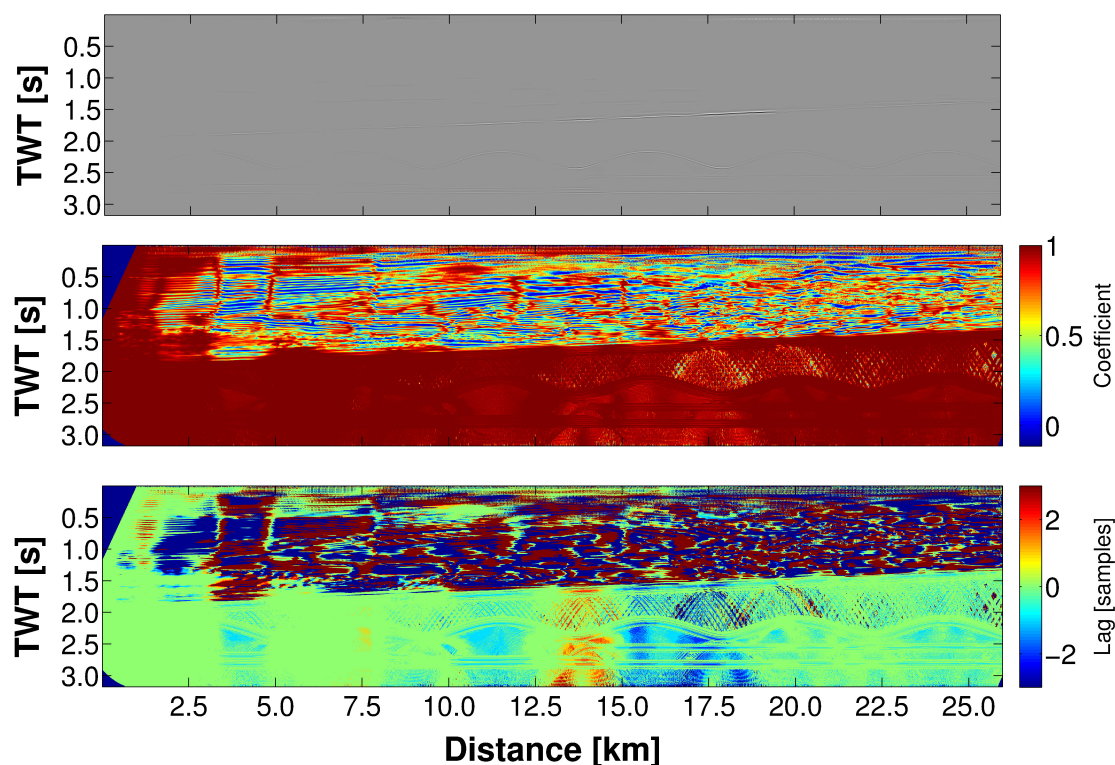


Figure 12: Results of the time-lag cross-correlation for the datasets DYN and STAT using a correlation window with a radius of 16 samples. The cross-correlation is performed only for the excerpt of the seismic section containing the subsurface reflections. The upper part shows the difference sections whereas the middle and lower part show the cross-correlation coefficient and the corresponding lag, respectively.

The results of the time-lag cross-correlation are shown in Fig. 12. The water column is characterized by a strongly differing correlation coefficient. The only exception is the area before 2.5 km since the dynamic and static section use the same water-velocity model in this area. The differences between the static and dynamic seismic section result in lags of up to ± 30 ms. The part of the seismic section containing the subsurface reflections looks different. For most parts of this area, the cross-correlation coefficient is above 90% whereas the most lags are in the range of -2 to 2 ms. A negative lag corresponds to a decrease in travel time due to denser water whereas a positive lag indicates an increase in travel time due to less dense water. Both cross-correlation coefficient and lag mirror the differences recognisable in the difference section in the upper part of Fig. 12 perfectly. The largest lags occur again between 12.5 and 20 km which corresponds to the area where the Mediterranean water mass moves along the slope. There is a strict separation between the areas with positive lags and those with negative lags, which is expected since variations in the water column at a certain position affect all of the underlying subsurface at that position in the same way. The only exceptions are on the right side of the seismic section above the sinusoidal reflector where it looks like some kind of cross-correlation noise is present. Furthermore, all the lags introduced in the area of the subsurface reflections result from the differences generated at the sea bottom and reach from the sea bottom reflection to the end of the section without differing much.

The time-lag cross-correlation is also performed for the high-frequency datasets. The results are presented in Figure 13. The same key features as in Fig. 12 are recognisable, but again, the differences and therefore the lags are more distinct than in the previous case. The results of the space-lag cross-correlation

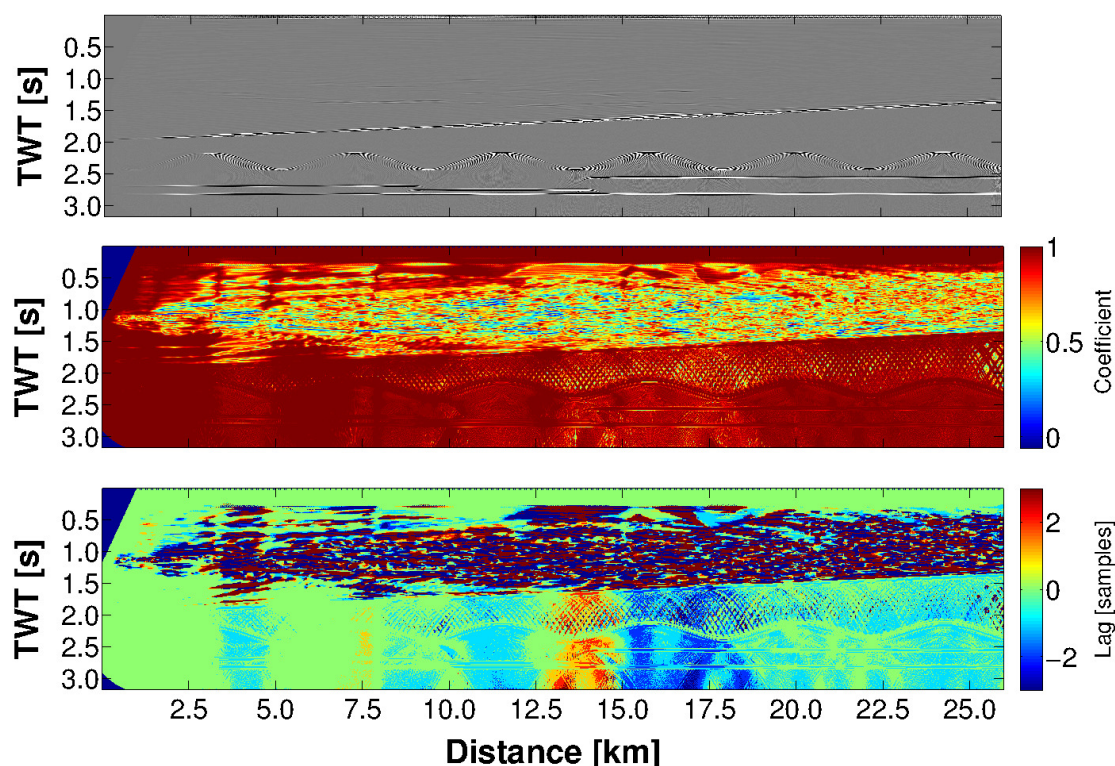


Figure 13: Results of the time-lag cross-correlation for the datasets DYN and STAT using a correlation window with a radius of 16 samples. For these datasets, the additional low-pass filter is not applied and the direct wave is still contained in the data. The cross-correlation is performed only for the excerpt of the seismic section containing the subsurface reflections. The upper part shows the difference sections whereas the middle and lower part show the cross-correlation coefficient and the corresponding lag, respectively.

are shown in Fig. 14. As in the case of the time-lag cross-correlation, the cross-correlation differs strongly for the water-column and large and numerous lags are introduced. In the area of the subsurface reflections, the smallest values of the cross-correlation coefficient (in the middle Fig. 14) and the largest lag values (in the lower part of Fig. 14) coincide with the areas showing the largest differences in the difference section at the top of the figure. In contrast to the time-lag cross-correlations, the lags are mostly restricted to the areas of the subsurface reflections. Furthermore, lags in space do not necessarily occur at every position where vertical lags are present (compare for example Fig. 12 and 14 at 7.5 km). Also, the lags in space are independent from the lags occurring at the sea bottom. As already shown in the case of the time-lag cross-correlation, the results for the datasets containing the higher frequencies are also more distinct in the case of the space-lag cross-correlations (see Fig. 15).

DISCUSSION AND CONCLUSIONS

An oceanographic model was used to assess the influence of ocean dynamics on time-lapse seismics. A synthetic seismic survey was performed where images for a static and dynamic ocean were compared. Several techniques were used to evaluate the quantitative and qualitative impact on the seismic data. Although differences between the dynamic and static section in the region of the subsurface reflections are not visible to the naked eye, the difference section revealed variations caused by the time-lag between the seismic sections that are in the same order of magnitude as the amplitudes of the reflections of the individual surveys. Areas of turbulent water mass behaviour are clearly distinguishable from areas with no water movement. The differences are more distinct when a broader frequency spectrum is used.

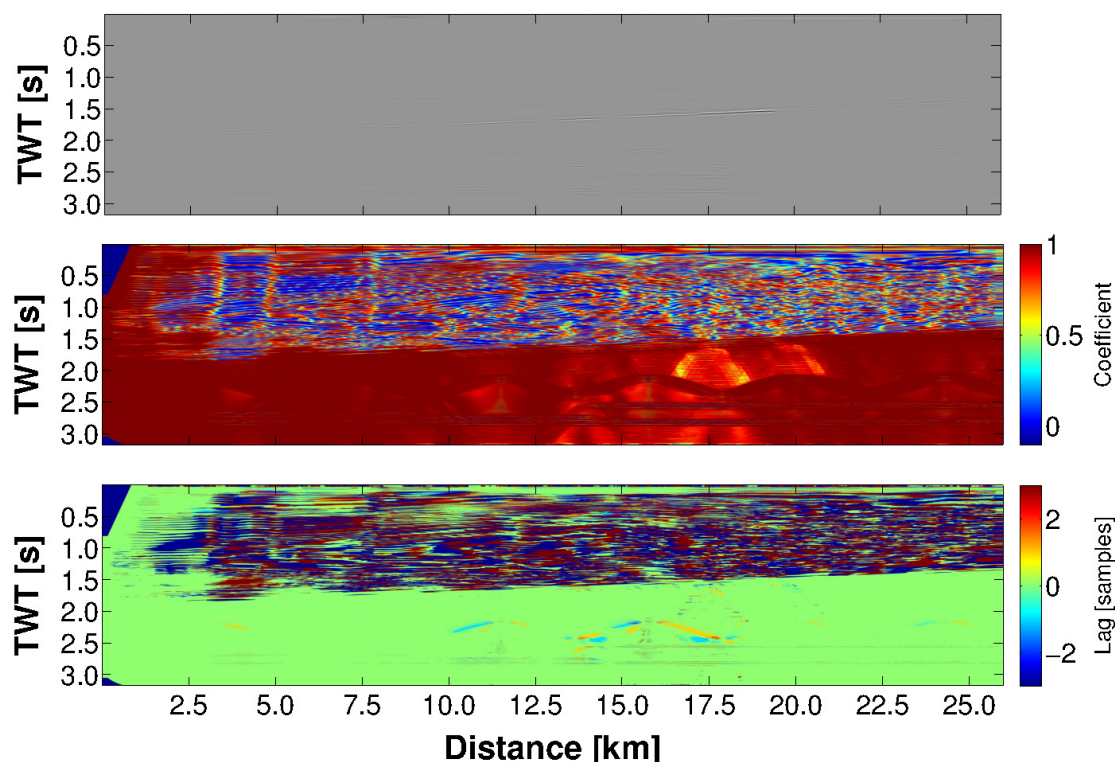


Figure 14: Results of the space-lag cross-correlation for the datasets DYN and STAT using a correlation window with a radius of 16 samples. The cross-correlation is performed only for the excerpt of the seismic section containing the subsurface reflections. The upper part shows the difference sections whereas the middle and lower part show the cross-correlation coefficient and the corresponding lag, respectively.

Kragh and Christie (2002) state that the NRMS value is extremely sensitive to the smallest changes in the data. If noise is present in the data, it will be strongly reflected in the NRMS error whereas the changes in the repeatability metric relate directly to the signal strength in the case of noiseless datasets. The NRMS metric reflects changes in reflectivity and noise and is sensitive to amplitude, phase, and static change. These statements are confirmed by the results of the repeatability metrics for the comparison of the dynamic and static datasets. In the case of the standard datasets, where no noise is present, the NRMS error curve is very sensitive to differences between the two datasets and these differences are easily recognisable in the NRMS error compared to much lower background values. If, however, random noise is added to the data, the NRMS values increase significantly and the peaks due to the differences in the data are hardly recognisable anymore. The results also confirm the statement of Bertrand and Thiebaud (2008) that higher frequencies promote the detection of subtle 4D changes. With increasing content of high frequencies in the frequency spectrum, the NRMS values increase as well. Furthermore, the resulting NRMS values of up to 60% are approximately in the same order of magnitude as those shown by Kragh and Christie (2002) and are much higher than those normally achieved for 4D surveys.

The results of the cross-correlation assert those obtained by the difference section and the NRMS values. The windowed cross-correlation using a radius of 16 samples reveals lags of up to 30 ms for the water column and of mostly 2 ms for the area of the subsurface reflections. Lags in the same size also occur in space. Again, the lags are more numerous and more distinct when using a broader frequency spectrum.

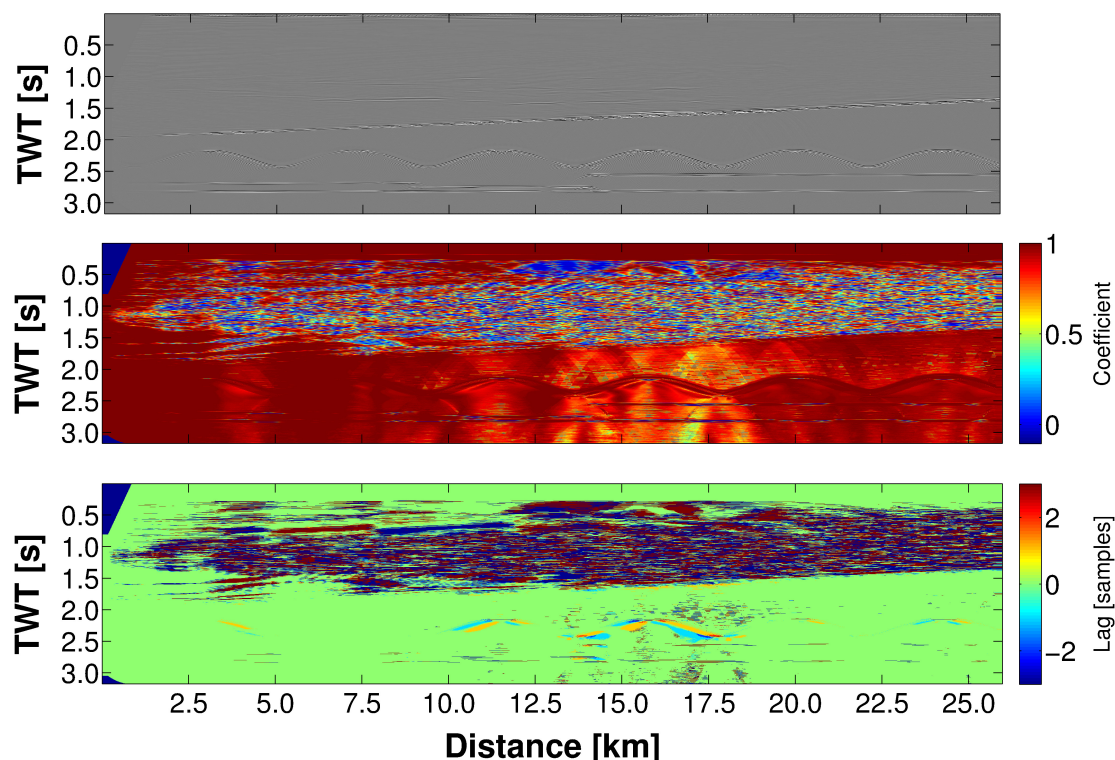


Figure 15: Results of the space-lag cross-correlation for the datasets DYN and STAT using a correlation window with a radius of 16 samples. For these datasets, the additional low-pass filter is not applied and the direct wave is still contained in the data. The cross-correlation is performed only for the excerpt of the seismic section containing the subsurface reflections. The upper part shows the difference sections whereas the middle and lower part show the cross-correlation coefficient and the corresponding lag, respectively.

Although the variations in the water column are only very small compared to the usual density contrasts in seismic exploration, they result in a significant reduction of the repeatability and introduce horizontal and vertical lags. Despite the fact that the Strait of Gibraltar shows particularly strong water column dynamics, the influence of a dynamic water column should not be neglected. Especially with the improvement in acquiring broadband marine seismic data and therefore higher frequencies, the possibility to detect even smaller time-lapse signals also increases.

ACKNOWLEDGMENTS

This work was kindly supported by the sponsors of the *Wave Inversion Technology (WIT) Consortium*, Karlsruhe, Germany. We would also like to thank Nuno Serra (KlimaCampus, University of Hamburg, Germany) for providing the data of the oceanographic model in a gridded form suitable for the seismic modelling. This work was partly supported by the Centre of Excellence 'Integrated Climate System Analysis and Prediction' CliSAP of the University of Hamburg, funded through the German Science Foundation (DFG EXC-177, flex pool project 08/1-013).

REFERENCES

- Bertrand, A. (2005). Velocity variations cause errors in seismic analysis. *Offshore*, pages 118–120.
- Bertrand, A. and MacBeth, C. (2003). Seawater velocity variations and real-time reservoir monitoring. *The Leading Edge*, 22(4):351–355.

- Bertrand, A. and MacBeth, C. (2005). Repeatability enhancement in deep-water permanent seismic installations: a dynamic correction for seawater velocity variations. *Geophysical prospecting*, 53(2):229–242.
- Bertrand, A. and Thiebaud, J. (2008). Detectability and time-shift estimation with high-resolution, time-lapse seismic. *The Leading Edge*, 27:636.
- Evensen, A. and Landrø, M. (2010). Time-lapse tomographic inversion using a gaussian parameterization of the velocity changes. *Geophysics*, 75(4):U29–U38.
- Hill, S., Marfurt, K., and Chopra, S. (2006). Searching for similarity in a slab of seismic data. *The Leading Edge*, 25(2):168–177.
- Houck, R. (2007). Time-lapse seismic repeatability – How much is enough? *The Leading Edge*, 26(7):828–834.
- Kosloff, D., Filho, A., Tessmer, E., and Behle, A. (1989). Numerical Solution of the Acoustic and Elastic Wave Equations by a New Rapid Expansion Method. *Geophys. Prospecting*, 37:383–394.
- Kragh, E. and Christie, P. (2002). Seismic repeatability, normalized rms, and predictability. *The Leading Edge*, 21(7):640–647.
- Lacombe, C., Butt, S., Mackenzie, G., Schons, M., and Bornard, R. (2009). Correcting for water-column variations. *The Leading Edge*, 28(2):198–201.
- Laws, R. and Kragh, E. (2002). Rough seas and time-lapse seismic. *Geophysical prospecting*, 50(2):195–208.
- MacKay, S., Fried, J., and Carvill, C. (2003). The impact of water-velocity variations on deepwater seismic data. *The Leading Edge*, 22(4):344–350.
- Marsh, J., Whitcombe, D., Raikes, S., Parr, R., and Nash, T. (2003). Bp's increasing systematic use of time-lapse seismic technology. *Petroleum Geoscience*, 9(1):7–13.
- Raub, C. (2011). Seismic imaging of the dynamic water column. Master's thesis, University of Hamburg.
- Raub, C., Gajewski, D., Tessmer, E., and Spickermann, D. (2012). Seismic imaging of the dynamic water column. Submitted.
- Rickett, J. and Lumley, D. (2001). Cross-equalization data processing for time-lapse seismic reservoir monitoring: A case study from the Gulf of Mexico. *Geophysics*, 66(4):1015–1025.
- Spetzler, J. and Kvam, Ø. (2006). Discrimination between phase and amplitude attributes in time-lapse seismic streamer data. *Geophysics*, 71(4):O9–O19.
- Spickermann, D. (2011). Stacking velocities from water column reflections. Bachelor's thesis, University of Hamburg.
- Stein, J., Bertrand, A., and Bannister, D. (2006). 4d seismic provides quantitative data. *Offshore*, 66(3).
- Vedanti, N., Pathak, A., Srivastava, R., and Dimri, V. (2009). Time Lapse (4D) Seismic: Some Case Studies. *Earth Science India*, 2:230 – 248.
- Yu, J. and Thiebaud, J. (2009). How Small Is a Small 4D Signal - A Model Study for 4D Resolution. *EAGE Conference & Exhibition - Amsterdam*.